Simplified modelling strategies to simulate the dynamic behaviour of R/C walls

Panagiotis Kotronis, Jacky Mazars

SIMPLIFIED MODELLING STRATEGIES TO SIMULATE THE DYNAMIC BEHAVIOUR OF R/C WALLS

PANAGIOTIS KOTRONIS* and JACKY MAZARS
Laboratoire Sols Solides Structures (C.N.R.S./I.N.P.G./U.J.F.) and R.N.V.O.
Domaine Universitaire B.P. 53, F-38041 Grenoble Cedex 9, France

A continuous damage model and different simplified numerical strategies are proposed to simulate the behaviour of reinforced concrete (R/C) walls subjected to earthquake ground motions. For 2D modelling of R/C walls controlled primarily by bending, an Euler multilayered beam element is adopted. For 3D problems, a multifibre Timoshenko beam element having higher order interpolation functions has been developed. Finally, for walls with a small slenderness ratio we use the Equivalent Reinforced Concrete model. For each case, comparison with experimental results of R/C walls tested on shaking table or reaction wall shows the advantages but also the limitations of the approach.

Keywords: Damage; multifibre beam; lattice; simplified models; shear walls.

1. Introduction

Simulating the nonlinear behaviour of reinforced concrete (R/C) walls subjected to severe ground motion is an important problem for the engineering community. Nonlinear dynamic analysis of complex civil engineering structures based on a detailed finite element model requires large-scale computations and involves delicate solution techniques. The need to perform parametric studies and the stochastic nature of the input accelerations necessitate simplified numerical modelling that reduces computational cost. However, constitutive models for concrete under cyclic loading have to be able to take into account some complex phenomena such as decrease in material stiffness due to cracking, stiffness recovery that occurs at crack closure and inelastic strains concomitant to damage. An optimum idealization is then needed i.e. one that is sufficiently fine and yet not too costly.

One of the main characteristic of the nonlinear behaviour of concrete under severe cyclic loading is damage. In order to simulate that we use a continuous damage model with two scalar damage variables, one for damage in tension and the other for damage in compression. Unilateral effect (differences in the behaviour

depending on the sign of the loading [Mazars *et al.*, 1990]) and stiffness recovery are also included. For 2D modelling of R/C walls whose behaviour is controlled primarily by bending we choose the classical 2D Euler beam theory. Beams are divided in several layers where 1D constitutive relationships for steel and concrete are implemented. For 3D problems, a multifibre Timoshenko beam element with higher order interpolation functions has been developed. The element is free of shear locking phenomena, takes into account deformations due to shear and can be coupled with 2D or 3D constitutive laws. Finally, when dealing with structures with a slenderness ratio far from the classical beam theory a more reliable representation of shear deformations and shear stresses has to be provided. One possibility in that respect — always within the family of simplified modelling strategies — is to use the Equivalent Reinforced Concrete model that makes use of lattice meshes for concrete and reinforcement bars. Comparisons with experimental results of R/C walls tested on shaking table or reaction wall show, for each case, the advantages but also the limitations of the approach.

2. A Continuous Damage Model for Concrete Under Cyclic Loading

A constitutive model for concrete under cyclic loading ought to take into account some observed phenomena, such as decrease in material stiffness due to cracking, stiffness recovery which occurs at crack closure and inelastic strains concomitant to damage. To simulate this behaviour we use a continuous damage model with two scalar damage variables one for damage in tension and one for damage in compression [La Borderie, 1991]. Unilateral effect and stiffness recovery (damage deactivation) are also included. Inelastic strains are taken into account thanks to an isotropic tensor. The total strain is given by

$$\mathring{\boldsymbol{\varepsilon}} = \mathring{\boldsymbol{\varepsilon}}^{\mathbf{e}} + \mathring{\boldsymbol{\varepsilon}}^{\mathbf{in}}, \tag{1}$$

$$\mathring{\boldsymbol{\varepsilon}}^{\mathbf{e}} = \frac{\langle\sigma\rangle_+}{E(1-D_1)} + \frac{\langle\sigma\rangle_-}{E(1-D_2)} + \frac{\nu}{E}(\sigma - Tr(\sigma)\boldsymbol{I}), \tag{2}$$

$$\mathring{\boldsymbol{\varepsilon}}^{\mathbf{in}} = \frac{\beta_1 D_1}{E(1-D_1)}\frac{\partial f(\sigma)}{\partial\sigma} + \frac{\beta_2 D_2}{E(1-D_2)}\boldsymbol{I}, \tag{3}$$

where:

$$\begin{cases} \mathrm{Tr}(\sigma) \in [0, +\infty) \rightarrow \dfrac{\partial f(\sigma)}{\partial\sigma} = \boldsymbol{I} \\ \mathrm{Tr}(\sigma) \in [-\sigma_f, 0) \rightarrow \dfrac{\partial f(\sigma)}{\partial\sigma} = \left(1 - \dfrac{Tr(\sigma)}{\sigma_f}\right)\boldsymbol{I}\,, \\ \mathrm{Tr}(\sigma) \in (-\infty, -\sigma_f) \rightarrow \dfrac{\partial f(\sigma)}{\partial\sigma} = 0.\boldsymbol{I} \end{cases} \tag{4}$$

with $\mathring{\boldsymbol{\varepsilon}}^{\mathbf{e}}$ the elastic strains, $\mathring{\boldsymbol{\varepsilon}}^{\mathbf{in}}$ the inelastic strains and σ the stress tensor. $\boldsymbol{I}$ denotes the unit tensor, $\mathrm{Tr}(\sigma) = \sigma_{ij}$ is the crack closure function and σ_f the crack closure

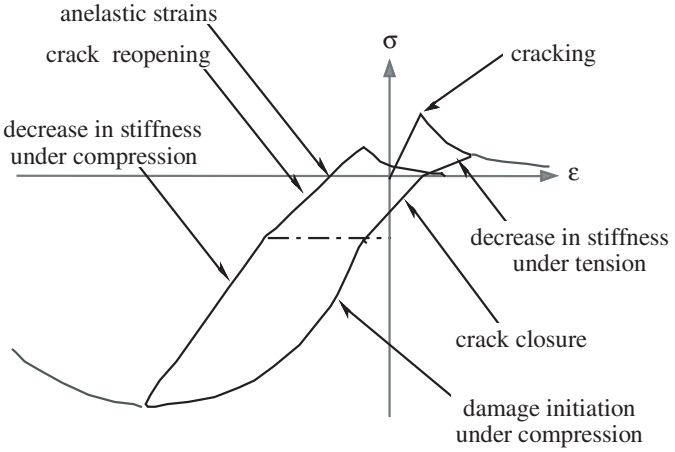

Fig. 1. Uniaxial response of the continuous damage model for concrete under cyclic loading.

stress. $\langle\cdot\rangle_+$ denotes the positive and $\langle\cdot\rangle_-$ the negative part of a tensor. E is the initial Young's modulus and ν the Poisson ratio. D_1 and D_2 are respectively the damage variables for traction and compression, β_1 and β_2 are material constants. Damage criteria are expressed as $f_i = Y_i - Z_i$ ($i = 1$ for tension or 2 for compression, Y_i is the associated force to the damage variable Z_i and Z_i a threshold dependent on the hardening variables). The evolution laws for the damage variables Z_i are written as:

$$D_i = 1 - \frac{1}{1 + \left[A_i \left(Y_i - Y_{0i}\right)\right]^{B_i}}, \tag{5}$$

where Y_{0i} = initial elastic threshold ($Y_{0i} = Z_i(D_i = 0)$) and A_i, B_i material constants. Figure 1 gives the stress-strain response of the model for a uniaxial traction-compression loading and Fig. 2 a sensibility study on the various parameters of the model using the following values: $E = 33\,500$ MPa, $Y_{01} = 3.3510^{-4}$ MPa, $Y_{02} = 1.5010^{-2}$ MPa, $A_1 = 4.00 \times 10^3\,\mathrm{MPa}^{-1}$, $A_2 = 7.00\,\mathrm{MPa}^{-1}$, $B_1 = 1.2$, $B_2 = 1.5$, $\beta_1 = 1.00$ MPa, $\beta_2 = -40$ MPa, $\sigma_f = 3.5$ MPa [La Borderie, 1991].

3. 2D Modelling of a R/C Wall

A simplified way to model a R/C wall whose behaviour is controlled primarily by bending is to use 2D multilayered Euler beam elements and concentrated masses at specific points (Fig. 3). Reinforcement bars are introduced within special composite layers, whose behaviour is obtained as a combination of those of concrete and steel according to:

$$\sigma_{layer} = (1 - \alpha_{rel})\sigma_{concrete} + \alpha_{rel}\sigma_{steel}, \tag{6}$$

where σ denotes axial stresses and α_{rel} is the relative area of the reinforcement in the layer. Uniaxial constitutive laws for concrete and steel are attributed at each layer and seismic loading is applied as an input motion at the base. Dynamic analysis for earthquake ground motion is done according to the classical Newmark

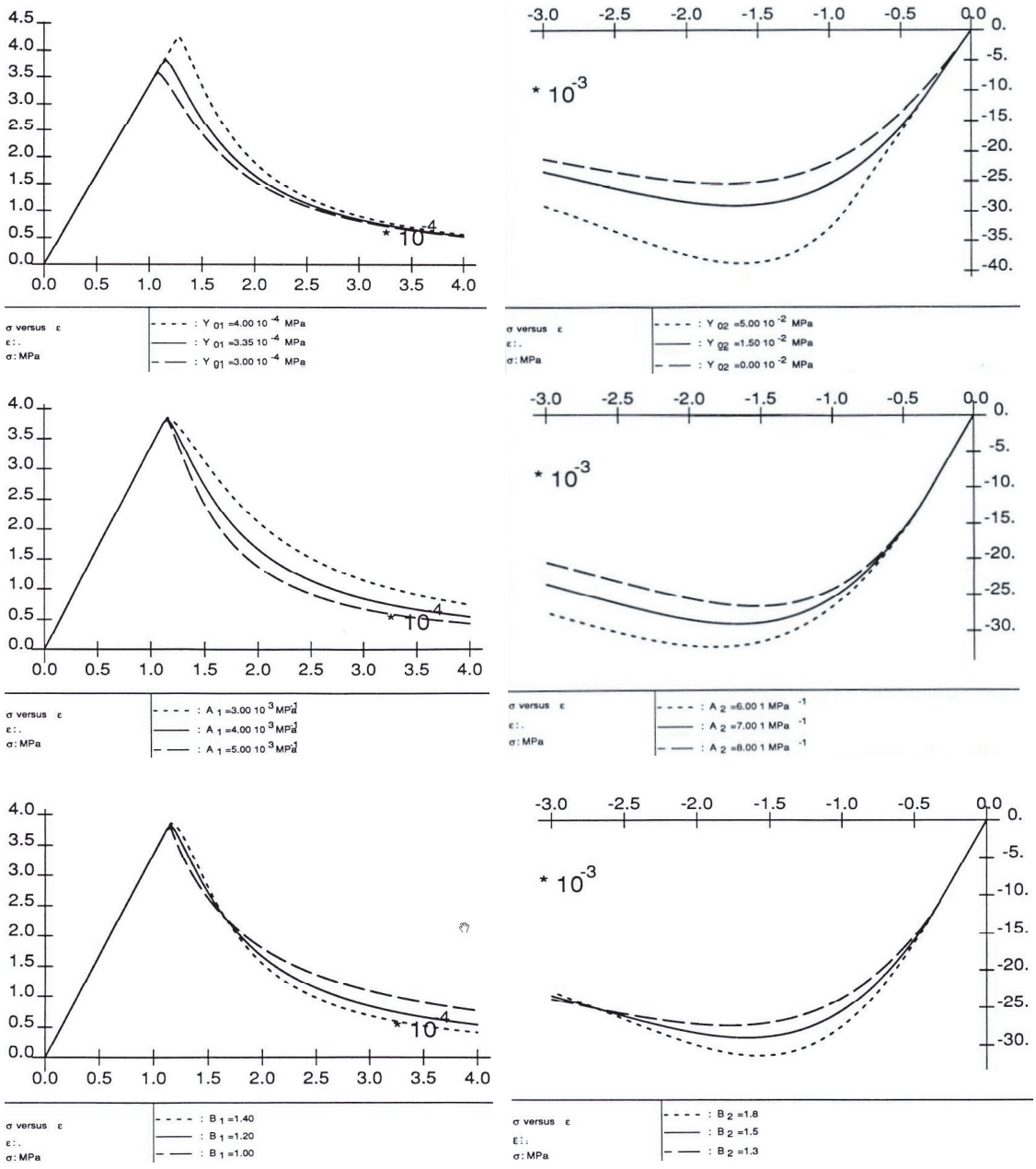

Fig. 2. Sensibility study on the various parameters of the continuous damage model for traction and compression [La Borderie, 1991].

scheme ($\gamma = 0.5$ and $\beta = 0.25$ are typically chosen for optimal result accuracy). The discrete set of equations obtained is further solved by an iterative Newton solution procedure, where at each iteration the secant stiffness matrix is used.

This approach has been used to model the nonlinear behaviour of the CAMUS III specimen tested on the shaking table at CEA Saclay [Combescure and Chaudat, 2000]. The 1/3rd scaled model is composed of two parallel 5-floor

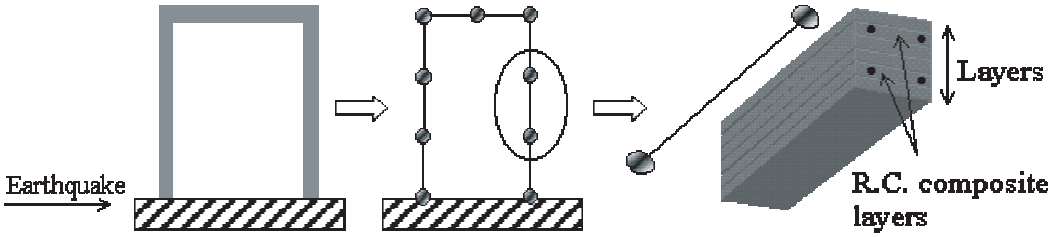

Fig. 3. Spatial discretisation of a R/C structure using 2D multilayered Euler beam elements.

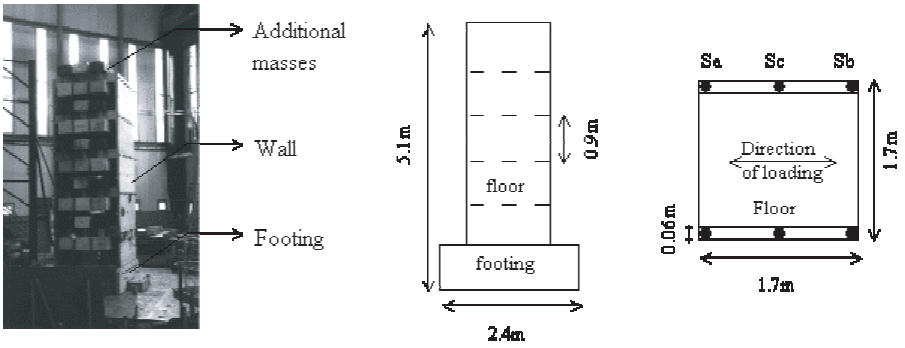

Fig. 4. CAMUS III — Characteristics of the specimen.

reinforced concrete walls without opening linked by 6 square floors. A highly reinforced footing allows the anchorage to the shaking table (Fig. 4). The total mass of the specimen is 36 000 kg. The mass of each floor, without the additional masses, is 1300 kg. The additional masses are determined in order to impose a normal force to the walls compatible with the vertical stress values commonly found at the base of such structures — 1.6 MPa in this case. The design philosophy follows EC8 provisions that privilege dissipation at a single flexural plastic hinge at the bottom of the structure. The rest of the wall is designed in order to avoid development of plastic behaviour anywhere above the base region (see Fig. 4 and Table 1). The target flexural capacity at the base of the specimen was equal to $M_{Sd} = 390$ kNm. Typical concrete mixtures were used for the casting of the specimen. Their characteristics were checked by the usual compressive and splitting tests. Tensile tests performed before the tests helped also to define the properties of the steel bars.

Table 1. CAMUS III — Steel reinforcement for each wall (mm^2).

CAMUS III		
	Sa, Sb	Sc
Level 5	132.4	159
Level 4	233	159
Level 3	233	159
Level 2	289.6	159
Level 1	289.6	159

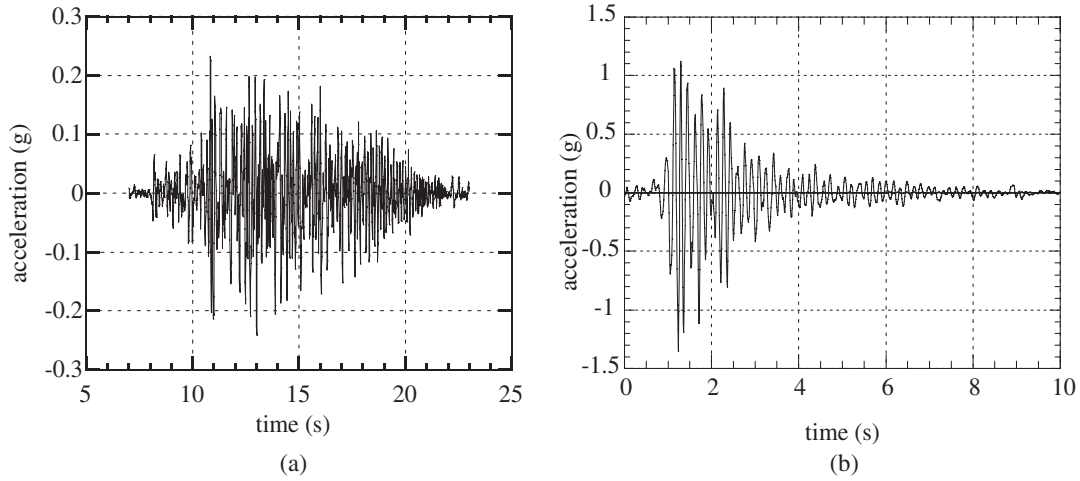

Fig. 5. CAMUS III — Ground motions: (a) Nice S1 — $a_{max} = 0.25\,g$; (b) Melendy Ranch — $a_{max} = 1.35\,g$.

During the shaking table tests the specimen was loaded with horizontal acceleration signals parallel to the walls in their own plane. Two types of ground motion were used: The artificial Nice S1 signal, representative of a far field earthquake and of the French design acceleration spectra and the Melendy Ranch signal representative of a near field earthquake (Fig. 5). Nice S1 is rich in terms of frequencies. Melendy Ranch is short and has a thin effective bandwidth of high accelerations. The frequency content of the Melendy Ranch signal is rich around 7 Hz, which was proven to be approximately the first natural frequency of the CAMUS III specimen (6.88 Hz). The dynamic tests were performed until collapse of the specimen. By collapse we mean the appearance of significant cracks on the concrete walls and plastic strain with possible failure of some bars of the vertical reinforcing steel.

During the first two sequences of the experimental campaign (Nice S1 — $0.42\,g$ and Nice S1 — $0.24\,g$) CAMUS III stayed practically in the elastic zone without any yielding of the steel bars. The following signal however (Melendy Ranch — $1.35\,g$) caused important damage to the specimen with extensive cracking and beginning of crushing at the wall extremities. Permanent displacements were observed at the end of the sequence, sign of residual cracks and significant yielding of the reinforcement bars. A large crack appeared throughout the base of each wall. Bending moment reached the value of the ultimate moment ($M_{Rd} = 400$ kNm: design flexural capacity for the selected curtailment of vertical bars). It is reminded that the maximum accelerations of the Melendy Ranch signal were around the first natural frequency of the specimen.

The experimental campaign was concluded with two more sequences (Nice S1 — $0.64\,g$ and Nice S1 — $1.00\,g$) that caused the collapse of the specimen (rupture of steel bars at the base). After the Melendy Ranch seismic input motion, the strain gages situated just above the level of the construction joint of the first floor of the CAMUS III specimen indicated high strain values at this level on the one hand,

and much lower values at the level corresponding to the 2nd and 3rd floor, on the other hand. Consequently damage seemed to be concentrated at the level of first storey with large plastic rotation at the base. This fact was confirmed by the inspection of the specimen after the failure test (Nice S1 — 1.00 g): Almost all the vertical steel reinforcement bars were broken and buckled just above the level of the 1st construction joint. The zone where rupture of the bars took place followed the main cracks at the base. A more detailed presentation covering all aspects of the experimental program can be found in Combescure and Chaudat [2000].

The 2D numerical model adopted represents each wall as a cantilever beam (Fig. 6). The wall is divided into 24 vertical Euler beam elements with 37 layers each. Concentrated masses are introduced at each floor (980 kg for the ground floor, 3119.5 kg for the fifth floor and 3226.5 kg for the others). A single wall is considered. Bond slip and confinement are not taken into account. The Rayleigh-based formulation damping coefficients are adjusted according to a white noise test performed before the experiment (2% on the two first modes). The uniaxial version of the continuous damage constitutive law is used for concrete and a classical uniaxial plasticity model with nonlinear kinematic hardening for steel [Armstrong and Frederick, 1966]. The properties of the materials used for the calculations are presented in Table 2.

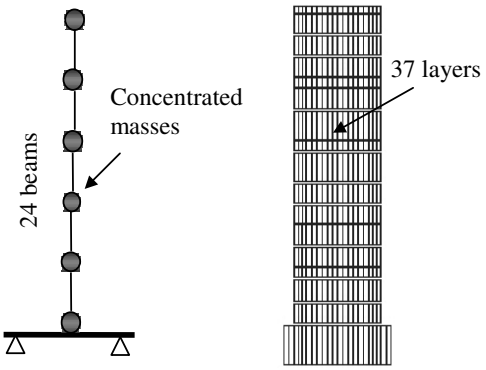

Fig. 6. CAMUS III (multilayered beam element) — Numerical model.

Table 2. CAMUS — Properties of the materials used for the numerical calculations.

CAMUS III		
Compression strength (concrete)	MPa	30
Tensile strength (concrete)	MPa	2.5
Young's modulus (concrete)	MPa	30 000
Young's modulus at the base (concrete)	MPa	15 000
Poisson coefficient (concrete)	—	0.2
Yield stress (steel)	MPa	414
Young's modulus (steel)	MPa	200 000

The Young's modulus of the base slab is taken smaller due to localised cracking already visible before the tests (those cracks appeared during the assembly of the specimens on the table particularly during the tightening of the wall anchorage to the floors).

Numerical results for two sequences of the experimental program (Nice S1 — $0.42\,g$ and Melendy Ranch — $1.35\,g$) are presented in Fig. 7. Due to an unreliable displacement transducer at the top of the specimen comparison of displacements is presented only at the fifth floor. No calibration of the numerical results has been

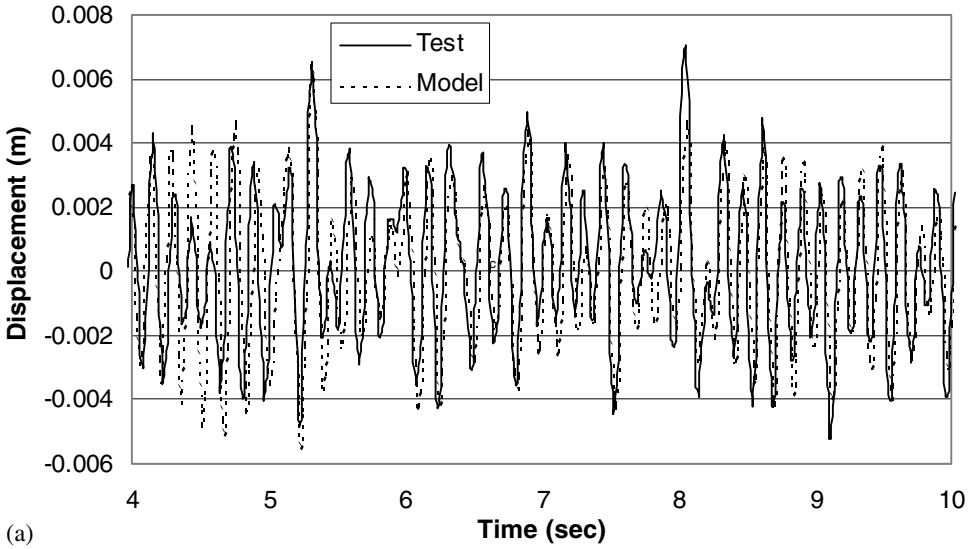

(a)

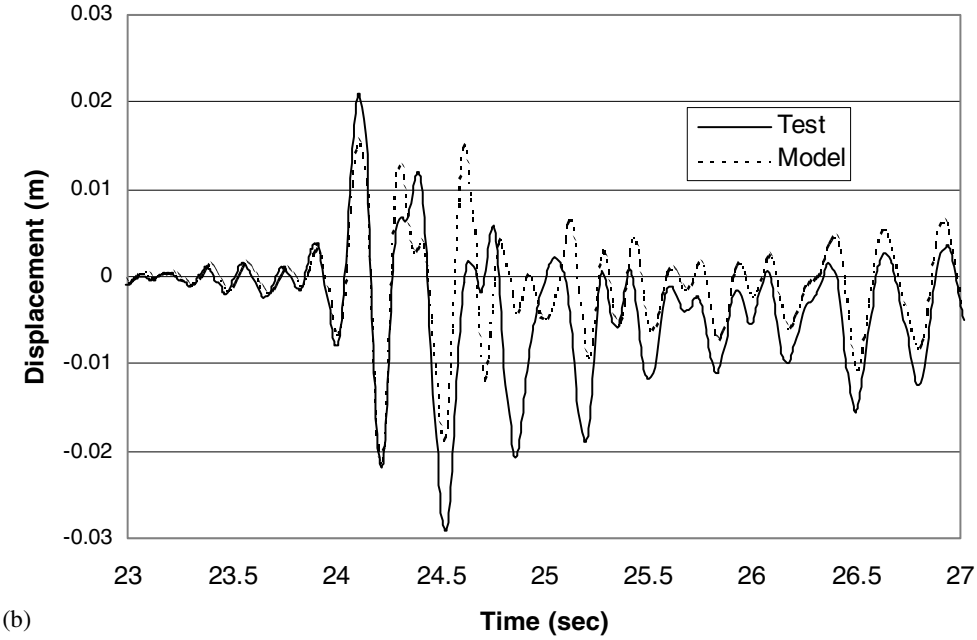

(b)

Fig. 7. CAMUS III (multilayered beam element) — Displacement time history at the fifth floor: (a) Nice S1 — $0.42\,g$; (b) Melendy Ranch — $1.35\,g$.

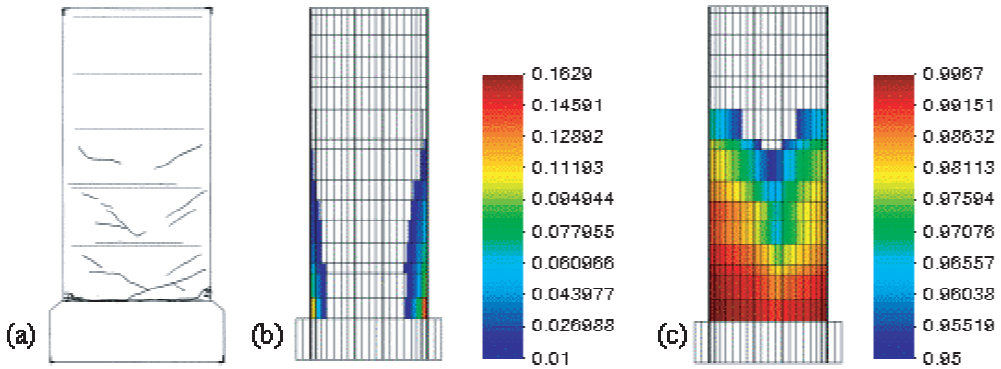

Fig. 8. CAMUS III (multilayered beam element) — Cracking of the wall at the end of the experiment. (a) Damage Pattern: Due to Compression — crushing after $D_2 \approx 0.15$; (b) due to Tension — cracking after $D_1 \approx 0.98$.

made, making the comparison with the experimental results similar to the one of "a blind simulation". Simulation predicts satisfactory the maximum displacement for both sequences and there is no shifting between the curves. The damage variables D_1 and D_2 in "Eq. (5)" vary normally between 0 (non damaged section) and 1.0 (completely damaged section). By filtering the value of D_1 between 0.95 and 1.0 we omit the micro-cracks and we have an image of the bigger cracks of the model. Figure 8 presents the damage pattern due to compression and tension at the end of the calculation for the complete loading program.

Comparison with the actual position of cracks shows that the model is able to reproduce the global trend observed experimentally (creation of the plastic zones at the base of the walls). The wall is mainly damaged at the base and that is in accordance with the EC8 design philosophy. For more detailed information and interpretation of the numerical results the reader is invited to look at [Kotronis, 2000] and [CAFEEL-ECOEST/ICONS, 2001].

4. 3D Modelling of a R/C Wall

In order to simulate — in a simplified manner — the 3D nonlinear behaviour of a R/C wall under dynamic loading, a 3D multifibre Timoshenko beam element has been developed [Kotronis, 2000] and [Kotronis *et al.*, 2004]. The difference with other multifibre Timoshenko beam elements usually found in the literature — [Guedes *et al.*, 1994; Spacone *et al.*, 1996; Petrangeli *et al.*, 1999] — is that the element is displacement-based and has higher order interpolation functions depending on the material's properties. It can be implemented to any general-purpose finite element code without major modifications. The user defines at each fibre a material and the appropriate constitutive law. The element takes into account deformations due to shear and uses cubic and quadratic Lagrangian polynomials for the transverse and rotational displacements respectively in order to avoid any shear locking

phenomena. The interpolation functions take the following form [Friedman and Kosmatka, 1993]:

$$\{U_s\} = [N]\{U\}, \tag{7}$$

$$\{U_s\}^T = \{u_s(x)\ v_s(x)\ w_s(x)\ \theta_{sx}(x)\ \theta_{sy}(x)\ \theta_{sz}(x)\}, \tag{8}$$

$$\{U\}^T = \{u_1\ v_1\ w_1\ \theta_{x1}\ \theta_{y1}\ \theta_{z1}\ u_2\ v_2\ w_2\ \theta_{x2}\ \theta_{y2}\ \theta_{z2}\}, \tag{9}$$

1 and 2 being the two nodes of the beam, x the axis of the beam, s the subscript defining "section variables", u, v, w the displacements and $\theta_x, \theta_y, \theta_z$ the rotations according to the x, y, z axis respectively (Fig. 9). $[N]$ is the matrix containing the interpolation functions:

$$[N] = \begin{bmatrix} N_1 & 0 & 0 & 0 & 0 & 0 & N_2 & 0 & 0 & 0 & 0 & 0 \\ 0 & N_3 & 0 & 0 & 0 & N_4 & 0 & N_5 & 0 & 0 & 0 & N_6 \\ 0 & 0 & N_3^* & 0 & -N_4^* & 0 & 0 & 0 & N_5^* & 0 & -N_6^* & 0 \\ 0 & 0 & 0 & N_1 & 0 & 0 & 0 & 0 & 0 & N_2 & 0 & 0 \\ 0 & 0 & -N_7^* & 0 & N_8^* & 0 & 0 & 0 & -N_9^* & 0 & N_{10}^* & 0 \\ 0 & N_7 & 0 & 0 & 0 & N_8 & 0 & N_9 & 0 & 0 & 0 & N_{10} \end{bmatrix}. \tag{10}$$

$$\begin{aligned}
N_1 &= 1 - \frac{x}{L}; \quad N_2 = \frac{x}{L}; \\
N_3 &= \frac{1}{1+\phi}\left\{2\Big(\frac{x}{L}\Big)^3 - 3\Big(\frac{x}{L}\Big)^2 - \phi\Big(\frac{x}{L}\Big) + 1 + \phi\right\}; \\
N_4 &= \frac{L}{1+\phi}\left\{\Big(\frac{x}{L}\Big)^3 - \left(2 + \frac{\phi}{2}\right)\Big(\frac{x}{L}\Big)^2 + \left(1 + \frac{\phi}{2}\right)\Big(\frac{x}{L}\Big)\right\}; \\
N_5 &= -\frac{1}{1+\phi}\left\{2\Big(\frac{x}{L}\Big)^3 - 3\Big(\frac{x}{L}\Big)^2 - \phi\Big(\frac{x}{L}\Big)\right\}; \\
N_6 &= \frac{L}{1+\phi}\left\{\Big(\frac{x}{L}\Big)^3 - \left(1 - \frac{\phi}{2}\right)\Big(\frac{x}{L}\Big)^2 - \frac{\phi}{2}\Big(\frac{x}{L}\Big)\right\}; \\
N_7 &= \frac{6}{(1+\phi)L}\left\{\Big(\frac{x}{L}\Big)^2 - \Big(\frac{x}{L}\Big)\right\}; \\
N_8 &= \frac{1}{1+\phi}\left\{3\Big(\frac{x}{L}\Big)^2 - (4+\phi)\Big(\frac{x}{L}\Big) + (1+\phi)\right\}; \\
N_9 &= -\frac{6}{(1+\phi)L}\left\{\Big(\frac{x}{L}\Big)^2 - \Big(\frac{x}{L}\Big)\right\}; \\
N_{10} &= \frac{1}{1+\phi}\left\{3\Big(\frac{x}{L}\Big)^2 - (2-\phi)\Big(\frac{x}{L}\Big)\right\},
\end{aligned} \tag{11}$$

with $N_i^* = N_i(\phi^*)$,ϕ and ϕ^* the stiffness ratios due to flexure and shear according to:

$$\begin{aligned}
\phi &= \frac{12}{L^2}\left(\frac{\int_S Ey^2\,dS}{k_y \int_S G\,dS}\right), \\
\phi^* &= \frac{12}{L^2}\left(\frac{\int_S Ez^2\,dS}{k_z \int_S G\,dS}\right).
\end{aligned} \tag{12}$$

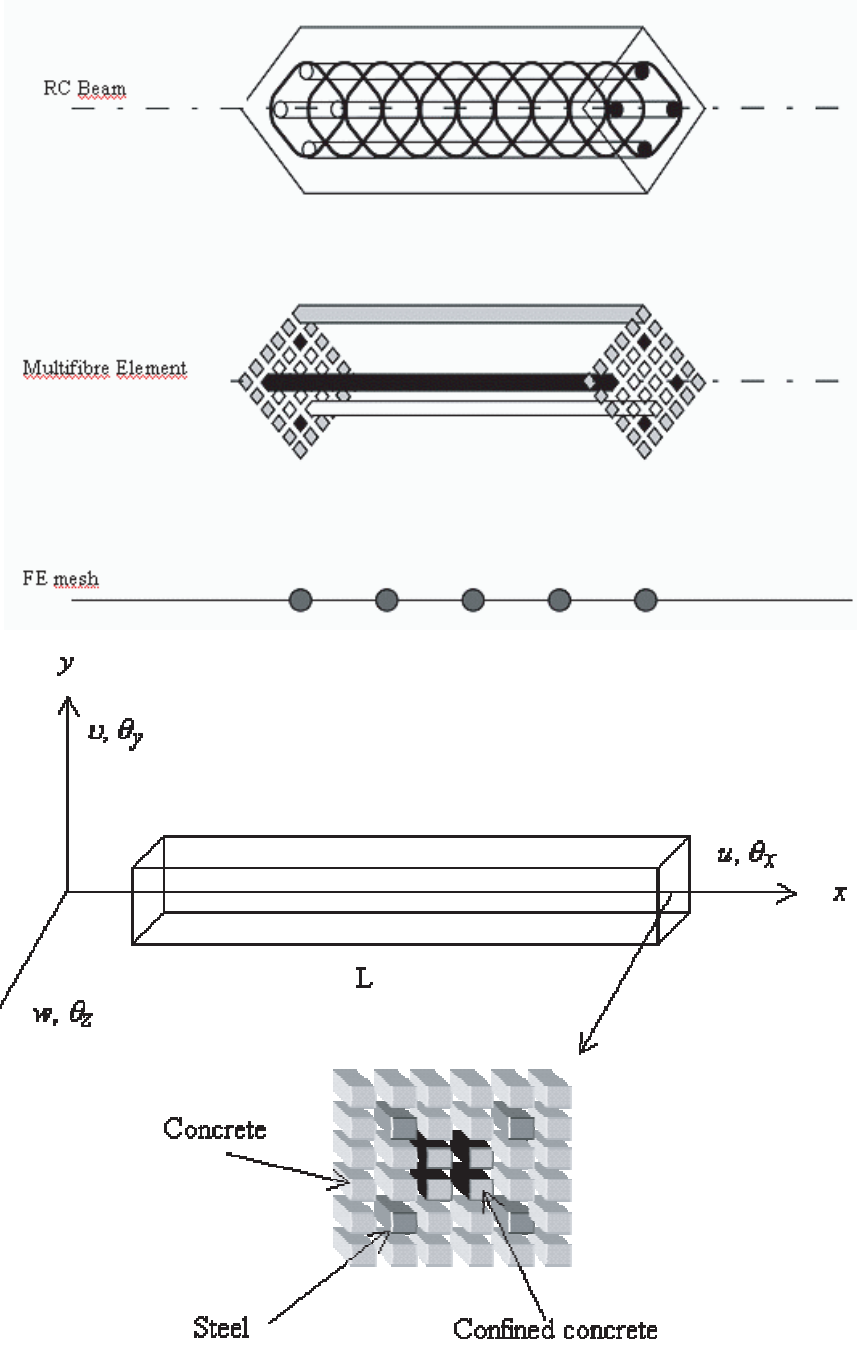

Fig. 9. Multifibre beam element for R/C structures.

L being the length and S the section of the beam, with k_y, k_z the shear correction factors dependent upon the material definition and cross-section geometry [Cowper, 1966], E and G are the Young's and shear moduli of the beam material. For slender structures ϕ and ϕ^* equal zero and the resulting stiffness and mass matrices are reduced to the ones of the Euler-Bernoulli beam theory. The interpolations functions depend on the materials properties and they are calculated only once, for the

first increment. If $\{F\}$ and $\{D\}$ are the section "generalised" stresses and strains respectively, the section stiffness matrix $[K_s]$ is calculated as [Guedes *et al.*, 1994]:

$$\{F\} = [K_s]\{D\}, \tag{13}$$

$$\{F\}^T = \{N\ T_y\ T_z\ M_x\ M_y\ M_z\}, \tag{14}$$

with N and T being the axial and shear forces respectively and M the moments.

$$\{D\}^T = \{[u_s'(x)]\ [v_s'(x) - \theta_{sz}(x)]\ [w_s'(x) + \theta_{sy}(x)]\ [\theta_{sx}'(x)]\ [\theta_{sy}'(x)]\ [\theta_{sz}'(x)]\}, \tag{15}$$

$$[K_s] = \begin{bmatrix} K_{s11} & 0 & 0 & 0 & K_{s15} & K_{s16} \\ & K_{s22} & 0 & K_{s24} & 0 & 0 \\ & & K_{s33} & K_{s34} & 0 & 0 \\ & & & K_{s44} & 0 & 0 \\ & & & & K_{s55} & K_{s56} \\ sym & & & & & K_{s66} \end{bmatrix}, \tag{16}$$

$$\begin{aligned} &K_{s11} = \int_S E\,dS; \quad K_{s15} = \int_S Ez\,dS; \quad K_{s16} = -\int_S Ey\,dS; \quad K_{s22} = k_y \int_S G\,dS; \\ &K_{s24} = -k_y \int_S Gz\,dS; \quad K_{s33} = k_z \int_S G\,dS; \quad K_{s34} = k_z \int_S Gy\,dS; \\ &K_{s44} = \int_S G(k_z y^2 + k_y z^2)\,dS; \quad K_{s55} = \int_S Ez^2\,dS; \quad K_{s56} = -\int_S Eyz\,dS; \\ &K_{s66} = \int_S Ey^2\,dS. \end{aligned} \tag{17}$$

The equation that gives the "generalised" strains as a function of the nodal displacements takes the following form:

$$\{D\} = [B]\{U\}, \tag{18}$$

$$[B] = \begin{bmatrix} N_1' & 0 & 0 & 0 & 0 & 0 & N_2' & 0 & 0 & 0 & 0 & 0 \\ 0 & N_3' - N_7 & 0 & 0 & 0 & N_4' - N_8 & 0 & N_5' - N_9 & 0 & 0 & 0 & N_6' - N_{10} \\ 0 & 0 & N_3'^* - N_7^* & 0 & -N_4'^* + N_8^* & 0 & 0 & 0 & N_5'^* - N_9^* & 0 & -N_6'^* + N_{10}^* & 0 \\ 0 & 0 & 0 & N_1' & 0 & 0 & 0 & 0 & 0 & N_2' & 0 & 0 \\ 0 & 0 & -N_7'^* & 0 & N_8'^* & 0 & 0 & 0 & -N_9'^* & 0 & N_{10}'^* & 0 \\ 0 & N_7' & 0 & 0 & 0 & N_8' & 0 & N_9' & 0 & 0 & 0 & N_{10}' \end{bmatrix}.$$

Finally, the stiffness matrix of the element is given by:

$$K_{elem} = \int_0^L B^T K_s B\,dx. \tag{19}$$

The implementation of the element was made in the library FEDEAS [Filippou, 1996] of the finite element code FEAP [Taylor, 2000]. In order to validate the performance of the proposed numerical strategy the experimental results of a R/C U

shaped wall tested pseudodynamically at the reaction wall of the ELSA laboratory at JRC Ispra were used [Pégon *et al.*, 2000]. The 3.6 m height — 1.0 scaled — specimen is composed of the U-shaped wall, a lower slab and an upper slab and its design follows EC8 provisions (Fig. 10). The upper slab is used as the horizontal load application point while six vertical post-tensioning bars apply a normal force of 2 MN. These bars are disposed in such a way that the force is applied close to the inertial centre in order to avoid spurious bending on the structure. Torsional rotation is prohibited during the tests. The total mass of the specimen is equal to 44 045 kg. The wall is loaded in both directions according to "the butterfly path" presented in Fig. 10.

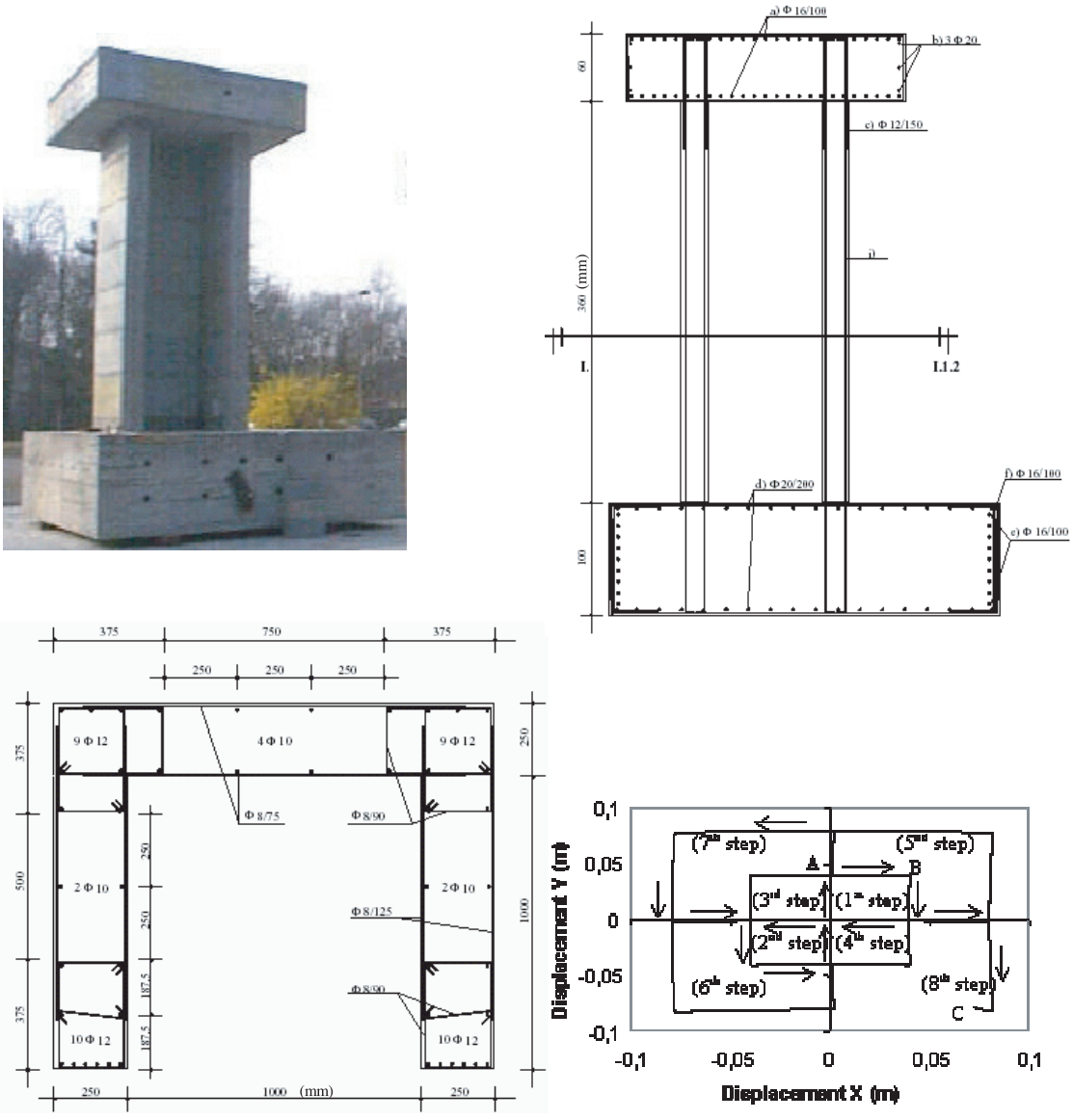

Fig. 10. U-shaped wall — Description of the specimen and loading history.

During the first butterfly cycle at 40 mm of the experimental campaign the structure mainly cracked and an important cyclic degradation was observed. During the cycle of 80 mm, large buckling and rupture of steels, spalling and severe degradation of concrete occurred. The structure collapsed at apex of larger magnitude of the last fly and was not pushed back to a zero displacement state. The U-shaped wall's "failure" in both directions occurred when three vertical steel bars broke straightening up back after buckling in compression [Pégon *et al.*, 2000].

Eleven multifibre Timoshenko beam elements are used for the numerical simulation of the U-shaped wall. 177 fibres simulate the concrete and 46 fibres the steel. Two Gauss points are considered at each element. Base slab is not simulated and the wall is considered fixed at the base. The behaviour of the top slab is linear elastic and rotation of the upper part is prohibited in order to reproduce correctly the boundary conditions of the test. The uniaxial version of the continuous damage constitutive law is used for concrete (shear and torsion are considered linear) and a classical uniaxial plasticity model with nonlinear kinematic hardening for steel. In order to take into account the influence of the stirrups the compression strength of the confined concrete is increased up to 30 MPa. The properties of the materials used for the calculations are presented in Table 3.

Comparison of numerical and experimental results for the eight steps of loading is represented in Fig. 11 (A, B, C letters refer to Fig. 10). One can observe the ability of the model to simulate relatively well the global behaviour of the specimen

Table 3. U-shaped wall — Properties of the materials used for the numerical calculations.

U-shaped wall	
Young's modulus (concrete)	28 900 MPa
Poisson coefficient (concrete)	0.25
Compression strength (concrete)	24 MPa
Compression strength (confined concrete)	30 MPa
Young's modulus (steel)	200 000 MPa
Poisson coefficient (steel)	0.3
Yield stress (steel)	515 MPa
Ultimate stress (steel)	615 MPa
Ultimate deformation (steel)	24%

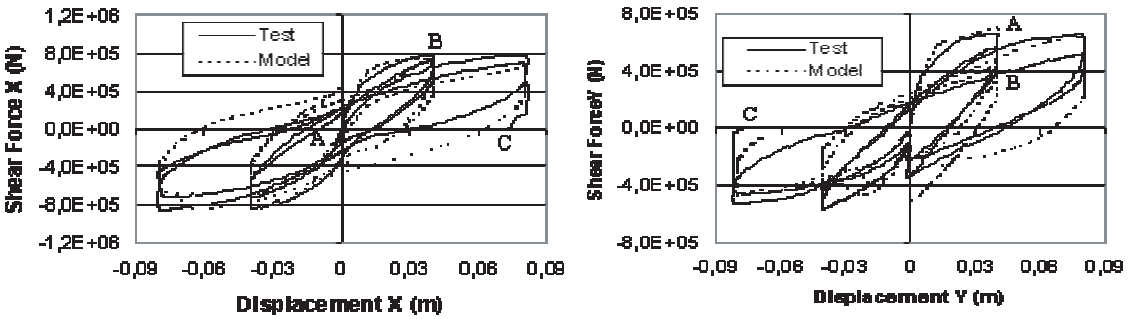

Fig. 11. U-shaped wall (multifibre beam element) — Experimental versus numerical results.

in terms of displacements and forces in both directions up to failure. However, the interpretation of the results is tedious since the specimen was mainly responding in shear to resist to high torsion moment and the fibre model is only taking into account elastic shear and torsion. The results at the global but also at the local level would be certainly improved with the implementation of a robust 2D or 3D constitutive model for concrete. Note also that the calculation is not time-consuming allowing for parametrical studies.

5. Modelling of a R/C Shear Wall with a Small Slenderness Ratio

A R/C shear wall of this kind is one that its behaviour is controlled primarily by shear. For structures with small slenderness ratio (less than 1) a model based on beam theory has difficulties in reproducing satisfactory shear deformations and stresses [Mazars *et al.*, 2002]. An alternative simplified method is the so-called Equivalent Reinforced Concrete model (ERC model) [Mazars *et al.*, 2002; Kotronis *et al.*, 2003]. The model uses a lattice mesh for predicting the nonlinear behaviour of shear walls under dynamic loading and is inspired on the Framework Method [Hrennikoff, 1941]. The basic idea consists of using the patterns of the Framework Method for 2D or 3D problems coupled with continuous damage mechanics in a nonlinear context and for a non-homogenous material. The main assumptions of the proposed strategy are (Fig. 12):

- An elementary volume of reinforced concrete (EV) can be separated into a concrete element (C) and a horizontal and a vertical reinforcement bar (S_H and S_V respectively). Concrete and steel are then modelled separately using two different lattices,
- The sections of the bars simulating concrete are derived from the Framework Method,

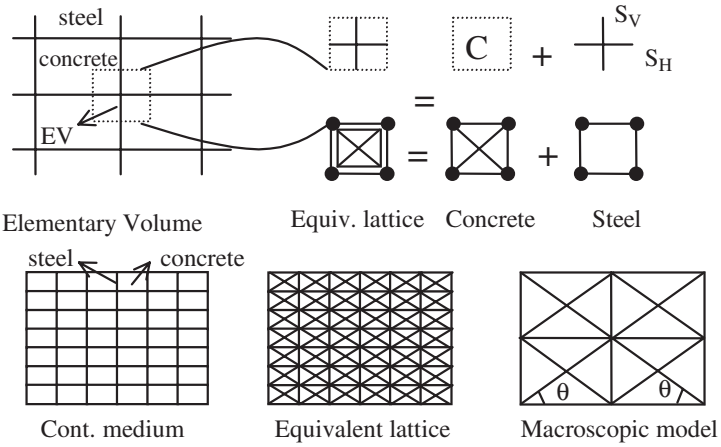

Fig. 12. The Equivalent Reinforced Concrete (ERC) model.

- A lattice composed by horizontal and vertical bars coupled with a uniaxial plasticity model with or without hardening simulates steel. The section and position of the bars coincide with the actual section and position of the reinforcement. In order to simplify the mesh the method of distribution is used, where the sections of bars are defined proportional to a corresponding surface area. In that way the mesh is independent of the geometry of the specimens,
- Perfect bond is assumed between concrete and steel,
- Geometrical symmetry of the pattern is required for cyclic and transient dynamic loading,
- For at least the type of structure tested hereafter, where the stress field is quite homogeneous, the number of elements that simulate concrete or steel does not have a great influence on the result [Kotronis, 2000]. Therefore a "macroscopic" model can be used instead of the "equivalent lattice" (Fig. 12).

The performance of the ERC model was evaluated on the NUPEC specimen (a shear wall with a slenderness ratio equal to 0.7, Fig. 13) tested on the shaking table at the Tadotsu Engineering Laboratory [OECD, 1996]. The objectives of the test were to comprehend the response characteristics of shear walls at levels ranging from the elastic state to the elasto-plastic ultimate state and to provide data for computer code improvement by comparing the results of computer analysis with the test results. The specimen was excited with horizontal acceleration signals (six sequences from RUN-1 to RUN-5) parallel to its plane (x direction, see Fig. 14). The rotation at the top of the specimen was free. The main characteristics of the specimen are presented in Table 4.

The pattern presented in Fig. 15 and the following equations of the Framework Method (valid for plane stress conditions) are used to calculate the lattice

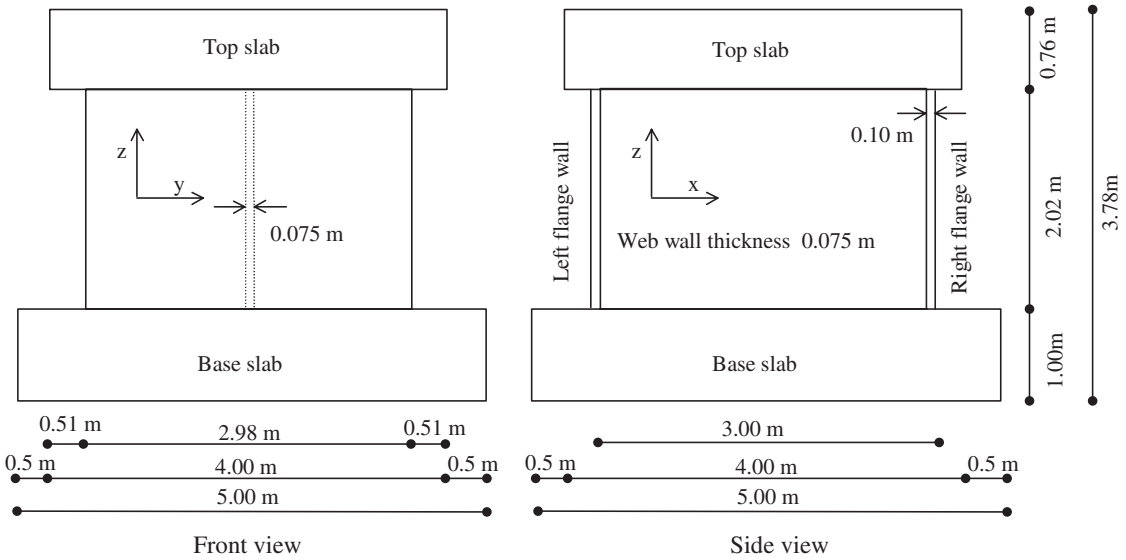

Fig. 13. NUPEC — Description of the specimen.

Table 4. NUPEC — Main characteristics of the specimen.

NUPEC		
Type of test		Dynamic on a shaking table
Boundary conditions		Rotation free at the top
Height/Length		≈ 0.7
Section of web wall	m^2	0.225
Section of flanges	m^2	0.596
Horizontal reinforcement	%	1.2
Vertical reinforcement	%	1.2
Compression strength of concrete	MPa	28.6
Tensile strength of concrete	MPa	2.3
Young's modulus of concrete	MPa	22 960
Yield strength of steel	MPa	384
Young's modulus of steel	MPa	188 000
Normal stress at the base	MPa	1.5
Mass (top slab + extra mass)	kg	$(29.1 + 92.9) * 10^3 = 122\,000$

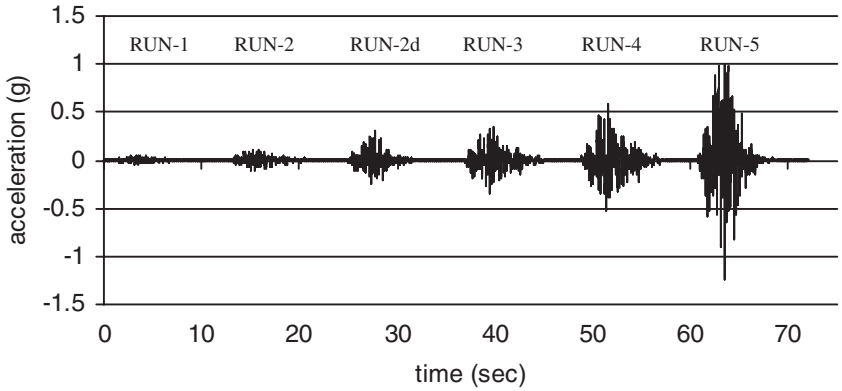

Fig. 14. NUPEC — Loading sequences.

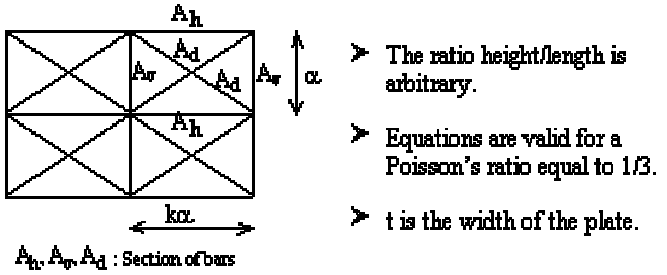

Fig. 15. Framework method — Pattern for plane stress.

simulating concrete:

$$A_v = \frac{3}{8}\,\frac{3k^2-1}{k}\alpha t, \tag{20}$$

$$A_h = \frac{3}{8}\,(3-k^2)\alpha t, \tag{21}$$

$$A_d = \frac{3}{16}\,\frac{(1+k^2)^{3/2}}{k}\alpha t, \tag{22}$$

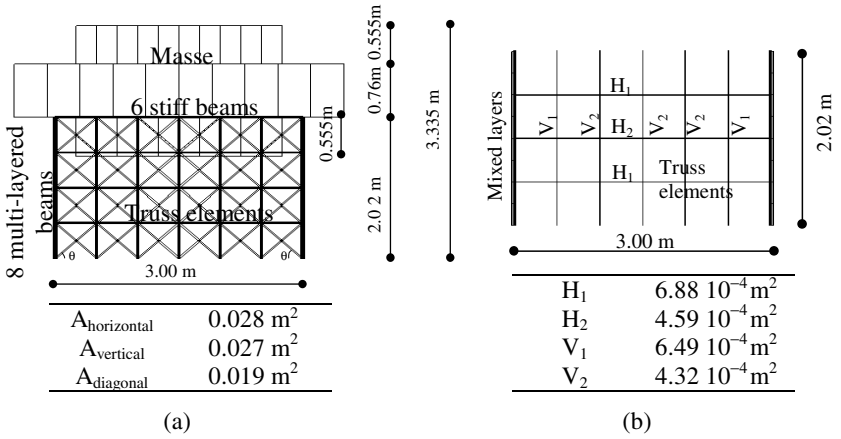

Fig. 16. NUPEC specimen (ERC model) — (a) Concrete mesh, (b) Steel mesh.

where k is the ratio between the length and the height α of the pattern and t is the width of the plate. The angle θ that the diagonals of the concrete lattice form with horizontal bars has been calibrated with the experimental results and it is found approximately equal to 45° (Fig. 16). Each flange is represented by eight multilayered beams (Euler-Bernoulli hypothesis) to account for possible flexure. The width of those beams equals the actual length of the flange (2.98 m). Six very stiff beams, free to rotate, simulate the top slab. Distributed masses are introduced at the top of the wall by three multilayered beams. Base slab is not simulated. Horizontal and vertical bars simulate horizontal and vertical reinforcement. Their sections and positions have been found by using the distribution method. Reinforcement in flanges is introduced through special mixed layers in the beams (Fig. 16). Parameters used for the materials are the ones already reported in Table 4.

A zoom at the last two sequences (RUN-4 and RUN-5, Fig. 17) shows that the ERC model predicts correctly the global behaviour of the NUPEC specimen in terms of maximum values and frequency content even under severe loading (just before collapse). A crucial parameter for the success of the nonlinear simulation is the angle θ that the diagonals of the concrete lattice form with the horizontal bars. This angle depends on the reinforcement ratios in the horizontal and vertical directions, the loading (normal compressive stress at the base of the specimens and shear stress) and the boundary conditions. It is related to the direction of the cracks into the structure (the bars are supposed reproducing the Ritter-Mörsch scheme). A parametrical study on the influence of this parameter can be found in [Kotronis *et al.*, 2003]. Results are also significantly improved by considering "the tension stiffening phenomenon" (tests on reinforced concrete elements demonstrated that even after extensive cracking, tensile stresses still existed in the cracked concrete and that they significantly increased the ability of the cracked concrete to resist shear stresses). Detailed information and interpretation of the numerical results can be found in [Kotronis, 2000].

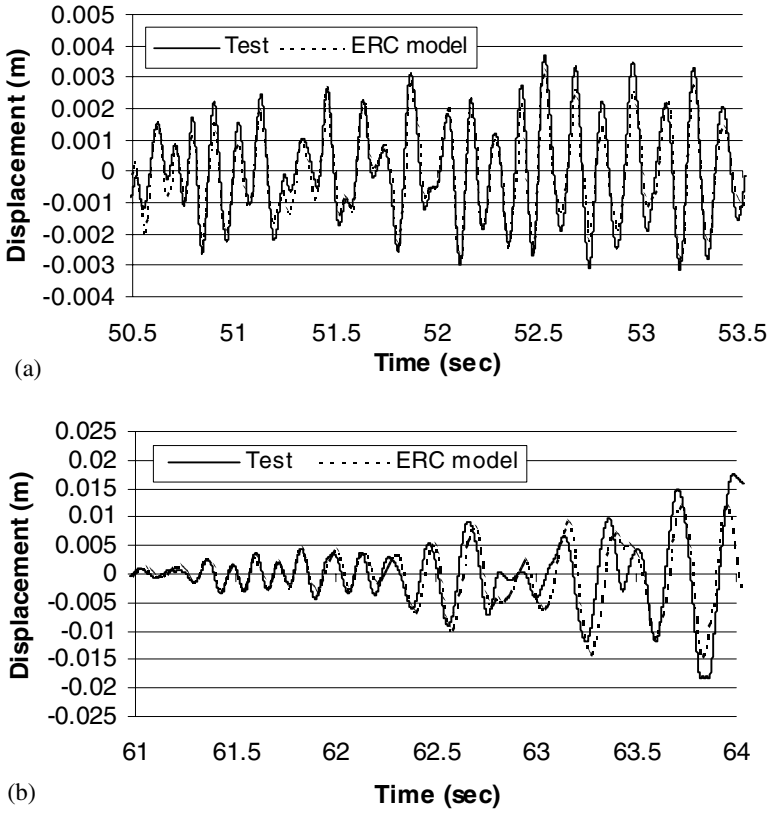

Fig. 17. NUPEC specimen (ERC model) — Displacement time history analysis: (a) RUN-4, (b) RUN-5.

6. Conclusions

In order to simulate correctly but also quickly the behaviour of R/C walls under severe ground motions one has to find the right compromise for an optimum idealisation i.e. one that is sufficiently fine and yet not too costly. Various simplified modelling strategies are presented in this work. Truss or beam type elements are used for the spatial discretisation coupled with a local constitutive law based on continuous damage mechanics. The advantage of using structural elements is that engineers are familiar with them and that the resulting mesh has a relatively small number of degrees of freedom. The multifibre or multilayered aspect is "transparent" to the user and complicates only the implementation stage of the elements in a finite element code. Nevertheless, in order to be able to reproduce complex nonlinear behaviours the constitutive law needs to be advanced enough to take into account complex phenomena as decrease in material stiffness due to cracking, stiffness recovery that occurs at crack closure and inelastic strains concomitant to damage. More specifically:

(i) For 2D R/C walls whose behaviour is controlled primarily by bending the use of Euler multilayered beam elements is a good compromise for an optimum

idealisation. Comparison with the experimental results of the CAMUS III program proves the ability of the proposed strategy to reproduce correctly the global but also the local behaviour of the specimen in terms of displacements, forces and damage distribution patterns. However, one has to keep in mind that a constitutive model based on a continuum mechanics theory has difficulties to reproduce discrete phenomena as the local behaviour of materials at areas were significant cracks appear. Due to the small reinforcement ratio of the CAMUS III specimen, failure phenomenon only can happen by rupture of the steel bars under tension, thus post-pick behaviour cannot be well represented. The lack of information at local scale (for example real strain in a steel bar at the location of a crack) is the major drawback preventing the designer from expressing physical criteria describing rupture. Furthermore, it is now well known that the use of local constitutive relationships provides results that are mesh-dependent. The use of a non-local damage model [Pijaudier-Cabot and Bažant, 1987] or a local second gradient model [Chambon *et al.*, 2001; Kotronis *et al.*, 2005] can provide a remedy in this particular problem.

(ii) In 3D problems where shear deformations are prevailing the use of multifibre Timoshenko beam elements is necessary. The proposed Timoshenko element has higher order interpolations functions, is free of shear locking phenomena and can be implemented to any general-purpose finite element code without major modifications. Numerical simulation of the U-shaped experimental program shows the ability of the element to simulate the global behaviour of the specimen even under severe loading. However, shear and torsion are considered linear for the calculations presented throughout this work (the 1D version of the constitutive continuous damage law is used). In order to reproduce correctly the behaviour at local level (for example in case of important warping) the implementation of a 3D robust constitutive law for concrete under cyclic loading is a necessary step. Another possibility in that respect is to consider a warping — conduction analogy method [Casaux *et al.*, 2004].

(iii) For structures with small slenderness ratio a model based on the Euler or Timoshenko beam theory has difficulties in reproducing satisfactory the shear deformations and stresses. A solution — always within the family of simplified models — is to use the Equivalent Reinforced Concrete model that privileges the use of two separate lattices meshes one for concrete and one for steel. A crucial parameter for the success of the nonlinear simulation is the angle that the diagonals of the concrete lattice form with the horizontal bars. Other limitations of the method are that perfect bond is assumed between concrete and steel — assumption also valid for the other two methods presented in this work — and the stress field must be quite homogeneous. Finally, although the extension of the method seems possible in 3D problems, its feasibility has still to be proven.

The most serious drawback of all the proposed strategies seems to be the use of a constant Rayleigh damping matrix. It seems likely that damping is not constant throughout the experiments but changes following the degradation of the structure. The proposed continuous damage model is not well suited to simulate this behaviour because it cannot dissipate energy under repeated cycles at constant loading amplitude. In order to remain within the framework of simplified methods recent developments investigated the possibility to extend the methods by introducing simple failure criteria and dissipation at a local (material) level in order to couple the state of cracking with the level of dissipation by frictional sliding of the crack surfaces [Ragueneau *et al.*, 2000].

Acknowledgements

The present work was granted from the European program ICONS [CAFEEL — ECOEST/ICONS, 2001].

References

Armstrong, P. J. and Frederick, C. O. [1966] "A mathematical representation of the multiaxial Bauschinger effect," *G.E.G.B. Report RD/B/N 731.*

CAFEEL-ECOEST/ICONS, [2001] "Thematic report N.5. Shear Walls Structures," editors J. M. Reynouard, M. N. Fardis, September.

Casaux, G., Ragueneau, F., Kotronis, P. and Mazars, J. [2004] "Enhanced 3D multifibre beam element accounting for shear and torsion," *Fifth International Conference on Fracture Mechanics of Concrete Structures*, Ia-FraMCos , Li *et al.* (eds.) **2**, 805–812.

Chambon, R., Caillerie, D. and Matsushima, T. [2001] "Plastic continuum with microstructure, local second gradient theories for geomaterials: Localization studies," *Int. J. Solids & Structures* **38**, 8503–8527.

Combescure, D. and Chaudat, Th. [2000] "ICONS European program seismic tests on R/C bearing walls. CAMUS III specimen," *Rapport DMT, SEMT/EMSI/TR/00-014/A*, CEA Saclay.

Cowper, G. R. [1966] "The shear coefficient in Timoshenko's beam theory," *ASME Journal of Applied Mechanics* **33**, 335–340.

Filippou, F. C. [1996] "Nonlinear static and dynamic analysis for evaluation of structures," *3rd European Conference on Structural Dynamics Eurodyn 96*, Florence, Italy, 395–402.

Friedman, Z. and Kosmatka, J. B. [1993] "An improved two-node Timoshenko beam finite element," *Computers and Structures* **47**(3), 473–481.

Guedes, J., Pégon, P. and Pinto, A. [1994] "A fibre Timoshenko beam element in CASTEM 2000," *Special publication Nr. I.94.31, J.R.C., I-21020*, Joint Research Center, Ispra, Italy.

Hrennikoff, A. [1941] "Solution of problems of elasticity by the Framework Method," *J. of Applied Mechanics*, A169–175.

Kotronis, P. [2000] "Cisaillement dynamique de murs en béton armé. Modèles simplifiés 2D et 3D," PhD thesis, Ecole Normale Supérieure de Cachan.

Kotronis, P., Mazars, J. and Davenne, L. [2003] "The equivalent reinforced concrete model for simulating the behaviour of shear walls under dynamic loading," *Engineering Fracture Mechanics* **70**(7–8), 1085–1097.

Kotronis, P., Davenne, L. and Mazars, J. [2004] "Poutre 3D multifibre Timoshenko pour la modélisation des structures en béton armé soumises à des chargements sévères," *Revue Française de Génie Civil* **8**(2–3), 329–343.

Kotronis, P., Chambon, R., Mazars, J. and Collin, F. [2005] "Local second gradient models and damage mechanics: Application to concrete," *ICFXI* — 11th *International Conference on Fracture*, Turin (Italy), March 20–25, (in print).

La Borderie, C. L. [1991] "Phénomènes unilatéraux dans un matériau endommageable: modélisation et application à l'analyse des structures en béton," PhD thesis, Université Paris 6.

Mazars, J., Berthaud, Y. and Ramtani, S. [1990] "The unilateral behavior of damaged concrete," *Engineering Fract. Mechanics* **35**(4–5), 629–635.

Mazars, J., Kotronis, P. and Davenne, L. [2002] "A new modelling strategy for the behaviour of shear walls under dynamic loading," *Earthquake Engineering and Structural Dynamics* **31**(4), 937–954.

OECD, [1996] "Seismic shear wall ISP. NUPEC'S seismic ultimate dynamic response test," Organisation for Economic-Cooperation and Development, Comparison report, OECD/GD(96)188.

Pégon, P., Plumier, C., Pinto, A., Molina, J., Gonzalez, P., Tognoli, P. and Hubert, O. [2000] "U-shaped-wall: Description of the experimental set-up," Report, Joint Research Center (J.R.C.), Ispra, Italy.

Petrangeli, M., Pinto, P. E., Ciampi, V. [1999] "Fiber element for cyclic bending and shear of RC structures. I: Theory," *J. Engrg. Mech.* **125**(9), 994–1001.

Pijaudier-Cabot, G. and Bažant, Z. P. [1987] "Nonlocal damage theory," *Journal of Engineering Mechanics* **113**, 1512–1533.

Ragueneau, F., La Borderie, C. and Mazars, J. [2000] "Damage model for concrete-like materials coupling cracking and friction, contribution towards structural damping: First uniaxial applications," *Mechanics of Cohesive-Frictional Materials* **5**(8), 607–626.

Spacone, E., Filippou, F. C. and Taucer, F. F. [1996] "Fiber beam-column model for nonlinear analysis of R/C frames. I: Formulation," *Earthquake Engineering and Structural Dynamics*, **25**(7), 711–725.

Taylor, R. L. [2000] "FEAP: A finite element analysis program, version 7.3 manual," University of California, Berkeley.